

Article

Abnormal Trend of Ferrite Hardening in a Medium-Si Ferrite-Martensite Dual Phase Steel

Ali Khajesarvi ¹, Seyyed Sadegh Ghasemi Banadkouki ^{1,*} , Seyyed Abdolkarim Sajjadi ² 
and Mahesh C. Somani ³ 

¹ Mining Technologies Research Center, Department of Mining and Metallurgical Engineering, Yazd University, Yazd 98195, Iran

² Department of Materials Science and Engineering, Ferdowsi University of Mashhad, Mashhad 91775, Iran

³ Materials and Mechanical Engineering, Centre for Advanced Steels Research, University of Oulu, 90014 Oulun Yliopisto, Finland

* Correspondence: sghasemi@yazd.ac.ir; Tel.: +98-913-3516-649

Abstract: In this paper, the effects of carbon, Si, Cr and Mn partitioning on ferrite hardening were studied in detail using a medium Si low alloy grade of 35CHGSA steel under ferrite-martensite/ferrite-pearlite dual-phase (DP) condition. The experimental results illustrated that an abnormal trend of ferrite hardening had occurred with the progress of ferrite formation. At first, the ferrite microhardness decreased with increasing volume fraction of ferrite, thereby reaching the minimum value for a moderate ferrite formation, and then it surprisingly increased with subsequent increase in ferrite volume fraction. Beside a considerable influence of martensitic phase transformation induced residual compressive stresses within ferrite, these results were further rationalized in respect of the extent of carbon, Si, Cr and Mn partitioning between ferrite and prior austenite (martensite) microphases leading to the solid solution hardening effects of these elements on ferrite.

Keywords: medium Si low alloy steel; step-quenched heat treatment; ferrite-martensite/ferrite-pearlite DP microstructure; alloying element partitioning; ferrite hardening variation



Citation: Khajesarvi, A.; Banadkouki, S.S.G.; Sajjadi, S.A.; Somani, M.C. Abnormal Trend of Ferrite Hardening in a Medium-Si Ferrite-Martensite Dual Phase Steel. *Metals* **2023**, *13*, 542. <https://doi.org/10.3390/met13030542>

Academic Editor: Andrea Di Schino

Received: 18 January 2023

Revised: 25 February 2023

Accepted: 6 March 2023

Published: 8 March 2023



Copyright: © 2023 by the authors. Licensee MDPI, Basel, Switzerland. This article is an open access article distributed under the terms and conditions of the Creative Commons Attribution (CC BY) license (<https://creativecommons.org/licenses/by/4.0/>).

1. Introduction

The low carbon, low alloy ferrite-martensite dual-phase (DP) steels are characterized by a mixture of soft ferritic matrix phase in conjunction with dispersed hard martensite. Attractive engineering properties are nowadays attained in these steels by the use of innovative heat treatments [1], which allow significant improvement in continuous yielding behavior, resulting in superior strength–ductility combinations in association with rapid strain hardening at early stage of plastic deformation due to the formation of a favorable microstructure [2–6]. These engineering properties are imparted by some of the variable microstructural parameters, such as ferrite and martensite volume fractions, their morphology and distribution, ferrite grain size, and the complex interaction of microphases with each other causing a considerable variation in mechanical behavior of low alloy DP steels [7–10]. Bag et al. [11,12] studied the impact and tensile properties of high martensite containing low alloy, ferrite-martensite DP steels and reported that an equal amount of finely divided ferrite and martensite microphases facilitate an optimum combination of high ductility and strength with good impact toughness. Using a 0.11% C, 1.6% Mn, 0.73% Si steel, Cai et al. [13] measured room temperature tensile properties of various samples with different ferrite and martensite morphologies, but with almost the same martensite volume fraction, derived from different primary microstructures. They reported that relatively higher strengths were attained in the DP samples, which received an intermediate quenching heat treatment, whereby the martensite content after intercritical annealing was very fine and fibrous morphology in the microstructures. Chang et al. [14] studied the effect of ferrite

grain size on the tensile properties of a low alloy DP steel and presented that the effect of ferrite grain size on the yield strength was much stronger than on the tensile strength.

A careful literature review of relevant articles regarding the structure-property relationships of low alloy DP steels indicate that the individual hardening behavior of ferrite and martensite microphases have been one of the noteworthy research topics in physical metallurgy of advanced high strength low alloy steels [15–17]. Kumar et al. [8] have reported that the ferrite hardness changed as a function of its volume fraction in a low alloy ferrite-bainite DP steel. They found that about 8% alteration in ferrite microhardness can be related with the ferrite-bainite DP samples consisting of 10 to 50% volume fraction of ferrite in conjunction with the remaining bainite regions. Another experimental work has also been conducted by Kumar et al. [8] showing that the mechanical behavior of low alloy ferrite-martensite DP steels was relevant to the size of ferrite grains. Also, the interaction between ferrite and martensite microconstituents has been believed to introduce unpinned dislocations generated within ferrite, which can affect the ferrite strain hardening in the low alloy ferrite-martensite DP steels [18,19]. Therefore, the ferrite hardening in ferrite-martensite DP steels has been presented to be variable depending on various parameters such as volume fraction, morphology and grain size of ferrite, and of course, the role of carbon and other alloying elements partitioning between ferrite and prior austenite (martensite) microphases are questionable and have been not followed significantly. Accordingly, it has been tried to find out the effect of carbon and other alloying elements partitioning on the ferrite hardening of different ferrite-martensite DP microstructures using a commercial grade of medium Si low alloy 35CHGSA steel by means of microhardness measurements and EDS analyses.

2. Materials and Methods

In the present investigation, a commercial grade of medium silicon low alloy 35CHGSA steel was used with the chemical composition indicated in Table 1. The heat treatment schedules were designed to achieve multiphase microstructures including various volume fractions of ferrite, pearlite, martensite and retained austenite microconstituents. The practical heat treatment processes practical the following sequential stages: (a) normalizing after austenitising at 900 °C for 15 min, (b) re-austenitising at 900 °C for 15 min to get fully homogenous prior austenite grains, (c) step-quenching (SQ) in a salt bath at 720 °C for 1–30 min to achieve different volume fractions of ferrite, and (d) rapid water quenching to transform all the remaining prior austenite to martensite. For each set of ferrite-martensite and ferrite-pearlite DP microstructure, three specimens were heat-treated in order to confirm the reproducibility of DP microstructures with respect to volume fractions of ferrite, pearlite, and martensite. In this way, the related specimens were marked as SQ1, SQ5, SQ15, and SQ30, representing the SQ holding times of 1, 5, 15 and 30 min, respectively, in salt bath maintained at 720 °C prior to water quenching. The applied heat treatment cycles are indicated schematically in Figure 1.

The metallography of heat-treated specimens was carried out on the transverse section surfaces relative to hot rolling direction of as-received strap specimens according to ASTM E 3 standard [20]. The polished specimens were etched with a 2% Nital solution (2 mL HNO₃ and 98 mL C₂H₅OH) [21] to reveal various microstructural features with good contrasting resolution. The ferrite, pearlite, and martensite volume fractions were measured according to the ASTM E562-02 standard [22]. The microstructural observations were carried out using a Olympus-PMG3 light microscope and a TESCAN-MIRA 3-XMU field-emission scanning electron microscope (FE-SEM) operating at an accelerated voltage of 15 kV. Both the spot and line scan energy dispersive X-ray spectroscopy (EDS) analysis techniques were largely applied to identify the carbon, Si, Cr and Mn concentrations in different locations of ferrite. Microhardness tests were conducted within ferrite, pearlite, and martensite microphases using a load of 5 g for ferrite grain and a somewhat higher load of 10 g for pearlite and martensite areas, applied for 20 s duration using a FM700 Future Tech microhardness tester, and the related data were presented as Vickers hardness numbers

(VHNs). In addition, microhardness tests were also carried out at different locations of select ferrite grains, but with a small load of 1 g applied for 20s duration loading time using a Future Tech microhardness tester machine model FM700. Two different locations of each step-quenched heat-treated samples were considered for conducting microhardness tests: (1) the central area of ferrite grain, and (2) the ferrite region close to the ferrite-martensite interfaces. The microhardness data were collected from at least five readings per sample, and the data were reported as Vickers hardness numbers (VHNs).

Table 1. The chemical composition of researched low alloy, medium silicon commercial grade of 35CHGSA steel (in wt%).

C	Si	Mn	Cr	S	P	Mo	Ni	Ti	V	Fe
0.35	1.25	0.89	1.18	0.01	0.01	0.01	0.04	0.03	0.01	Balance

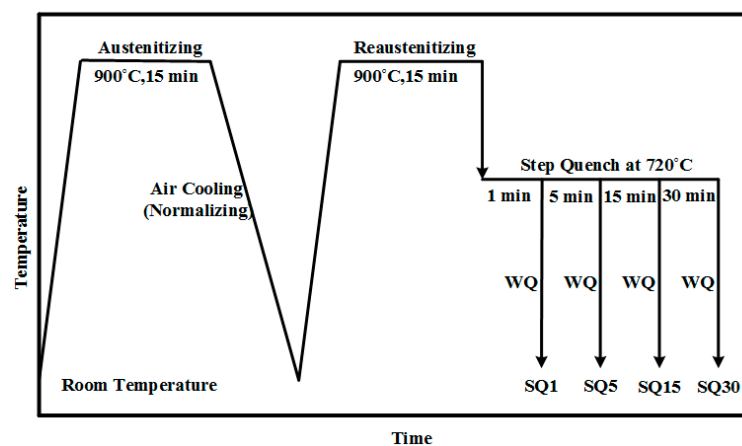


Figure 1. The schematic diagrams indicating heat treatment cycles used to achieve microstructures involving different volume fractions of ferrite, pearlite and martensite microphases. WQ: water quench; SQ: step quench [10].

The X-ray diffraction analysis was also carried out on a AW-DX300 Aseware X-ray diffractometer using copper $K\alpha$ radiation (1.54184 Å) and angular step size (in 2θ) of 0.05 degrees with a time step of 1 s. The residual stresses were quantified using the $\sin^2\Psi$ analysis technique [23,24]. The following expression was used to calculate the amount of residual stress within various SQ specimens [24]:

$$\frac{d_{\phi\Psi} - d_0}{d_0} = \frac{1 + \nu}{E} \sigma_{\phi} \sin^2 \Psi - \frac{\nu}{E} (\sigma_{11} - \sigma_{22}) \quad (1)$$

where $d_{\phi\Psi}$ is the d-spacing of diffracted planes oriented at an angle Ψ from the surface normal, d_0 is the d-spacing of (hkl) planes at $\Psi = 0$ deg, ν is poisson's ratio, E is young's modulus, σ_{11} and σ_{22} are principal stresses parallel to the surface, and σ_{ϕ} is the stress acting in a chosen direction of surface at an angle ϕ from σ_{11} . The σ_{ϕ} factor accounts for differences in specimen orientation, and is related to σ_{11} and σ_{22} parameters. The term $(\sigma_{11} - \sigma_{22})$ is constant for a given specimen, and Equation (1) shows that a linear variation between $d_{\phi\Psi}$ and $\sin^2 \Psi$ is expected [23]. The term $(d_{\phi\Psi} - d_0)/d_0$ can be plotted against $\sin^2 \Psi$ for several Ψ angles for a particular diffracted plane, and, the stress σ_{ϕ} can be calculated from the slope. When, the deviation of d with $\sin^2 \Psi$ data occurs, the residual stress can be determined using additional mathematical and experimental treatments.

3. Results and Discussion

3.1. Microstructural Characterization

Figure 2 represents typical light microstructures along with super imposed electron micrographs (at top right hand side) of SQ specimens heat-treated at 720 °C for various holding times. These micrographs show a significant increase in volume fraction, polygonality, grain size, and continuity of ferrite as a consequence of longer isothermal holding time at 720 °C. For more information, the progress of prior austenite decomposition in various SQ heat-treated specimens was measured in term of microconstituent volume fractions, and the associated results are given in Table 2. A careful microstructural analysis indicated that the microstructures of SQ1, SQ5, and SQ15 heat-treated samples were characterized by just a mixture of ferrite and martensite microphases, introducing ferrite-martensite DP microstructures, while in the case of SQ30 heat-treated samples, a maximum volume fraction of 15% ferrite along with the remaining 85% pearlite microconstituents formed in the microstructures, representing the typical ferrite-pearlite DP microstructures. In other words, with the increase in SQ holding time up to 30 min in the intercritical $\alpha+\gamma$ region, there was enough time available for carbon atoms to diffuse from ferrite into the prior austenite and equilibrate and this enabled enough carbon concentration within the prior austenite regions for subsequent pearlite formation.

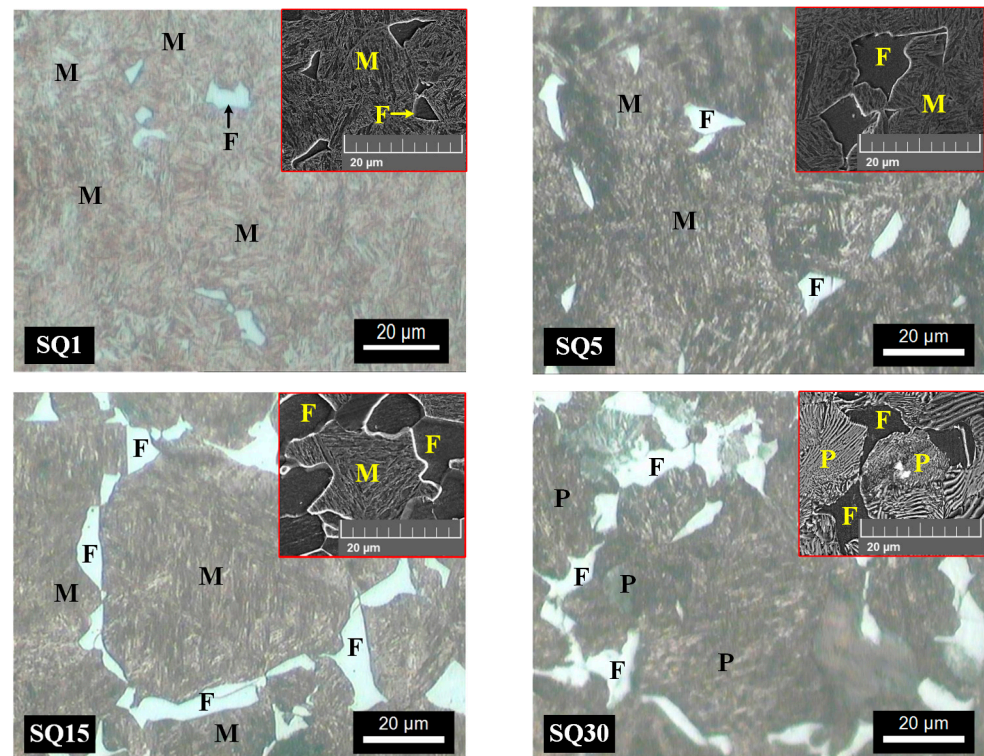


Figure 2. Light and FE-SEM micrographs of various SQ heat-treated specimens depicting the formation of ferrite, pearlite, and martensite microphases in the microstructures. The blocky ferrite grains were mostly surrounded by martensite areas in the SQ1 and SQ5 heat-treated specimens, while continuous grain boundary ferrite was developed in the SQ15 and SQ30 heat-treated samples. Microstructural features were characterized by ferrite-martensite DP microconstituents for SQ1, SQ5, and SQ15 samples, while ferrite-pearlite microphases were formed in the SQ30 heat-treated ones. Ferrite, pearlite, and martensite microconstituents are marked with F, P, and M symbols, respectively.

Table 2. The progress of ferrite and pearlite formations realized at 720 °C for various SQ holding times. The pearlite formation started after 15 min isothermal holding time.

Sample Mark	SQ Holding Time (min)	Ferrite Volume Fraction (%)	Martensite Volume Fraction (%)	Pearlite Volume Fraction (%)
SQ1	1	3	97	-
SQ5	5	6	94	-
SQ15	15	13	87	-
SQ30	30	15	0	85

3.2. Ferrite Hardening Variation

The alteration of ferrite hardening as a function of SQ holding time in conjunction with the changes in ferrite volume fraction, are illustrated in Figure 3. Figure 3a illustrates that the progress of ferrite formation can be characterized with a typical S-shaped curve indicating that the phase transformation of prior austenite to ferrite can be rationalized by a general diffusional nature of nucleation and growth for ferrite formation during SQ holding at 720 °C. The variation of ferrite grain size against SQ holding time is indicated in Figure 3b. The abnormal trend in ferrite hardness as a function of SQ holding time is illustrated in Figure 3c. Accordingly, the ferrite microhardness initially decreased from 352 to 217HV5g with the increase in SQ holding time from 1 to 15 min, beyond which it surprisingly increased to 245HV5g with further increase in SQ holding time to 30 min. It is interesting to emphasize that the minimum ferrite microhardness occurred in the ferrite-martensite DP specimens SQ15 consisting of 13% ferrite volume fraction with remainder phase fraction as martensite, and subsequent increase in ferrite hardness was realized for the SQ30 samples with essentially ferrite-pearlite microstructures. The minimum ferrite hardening response can be fully supported by the verity that the SQ heat treatment at longer holding time can be related to the more ferrite formation, in addition to the occurrence of significantly thermally activated relaxation, which decreases the accumulation of transformational residual stresses causing a lower hardness level in ferrite. In addition to the occurrence of these ferrite softening phenomena during longer holding times at 720 °C, the abnormal higher ferrite hardness realized in SQ30 samples suggests that another ferrite hardening mechanism must be operational, such as solid solution hardening effects caused by diffusion of substitutional alloying elements leading to simultaneous hardening of ferrite during the progress of its formation.

To examine the hardening alteration of ferrite grains more precisely, the microhardness test has been accomplished at different locations within certain ferrite grains using various SQ heat-treated samples. Typical light optical micrograph in Figure 4 shows an example of microhardness method followed, indicating indentation impressions taken from various positions (the central regions of ferrite grains and the ferrite regions adjacent to the ferrite-prior austenite interfaces) of ferrite grains using SQ5 heat-treated samples. It is obvious that the minimum ferrite microhardness has been associated to the central location of ferrite grains, and it increases as the microhardness test location is moved towards ferrite-prior austenite interfaces, thus clarifying that the deformation resistance of ferrite is related to the position of microhardness testing location. Therefore, as the microhardness location is moved from the central location of ferrite grains towards the ferrite area adjacent to the ferrite-prior austenite interfaces, the average ferrite microhardness increased from 122 to 145HV1g for the SQ5 specimens.

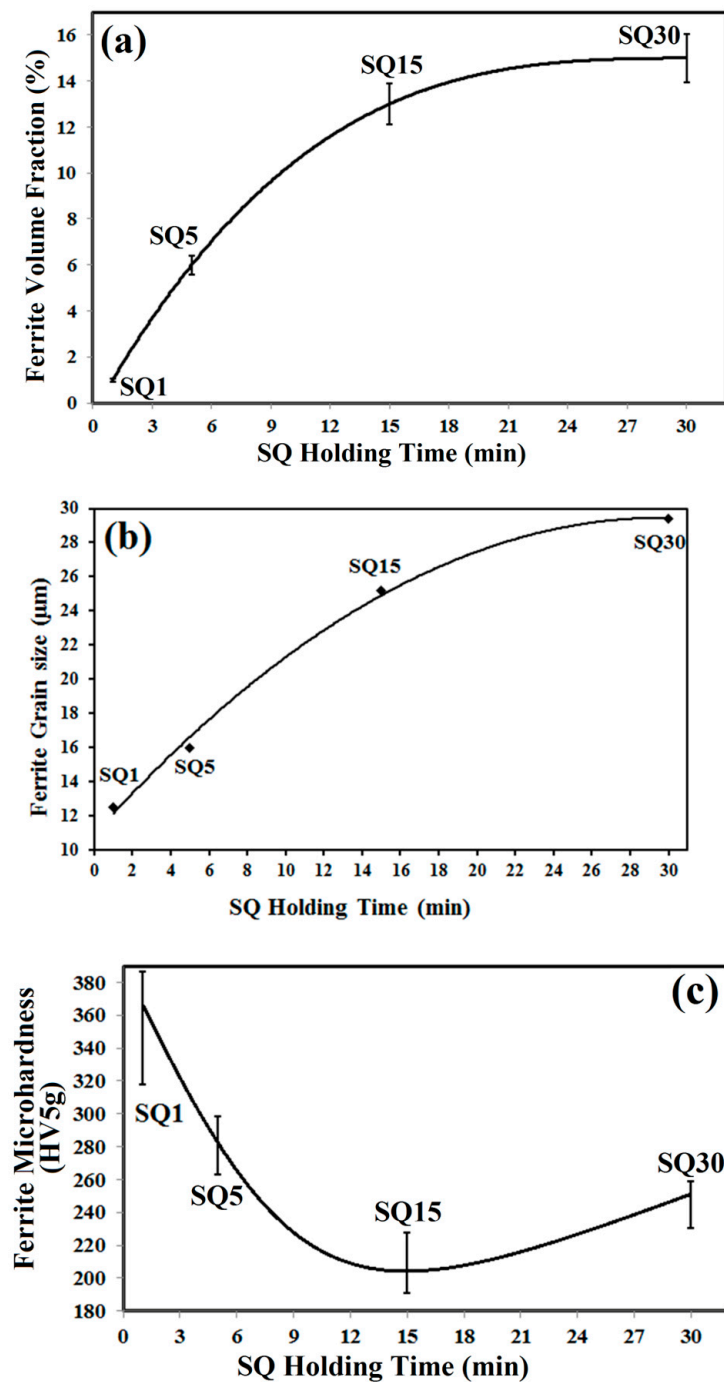


Figure 3. Changes in: (a) volume fraction of ferrite as a function of SQ holding time; (b) ferrite grain size against SQ holding time; and (c) ferrite microhardness versus SQ holding time. An abnormal trend in respect of ferrite hardening occurred during the progress of ferrite formation in the SQ30 heat-treated samples. The ferrite microhardness measurements are related with a fixed loading force of 5 g.

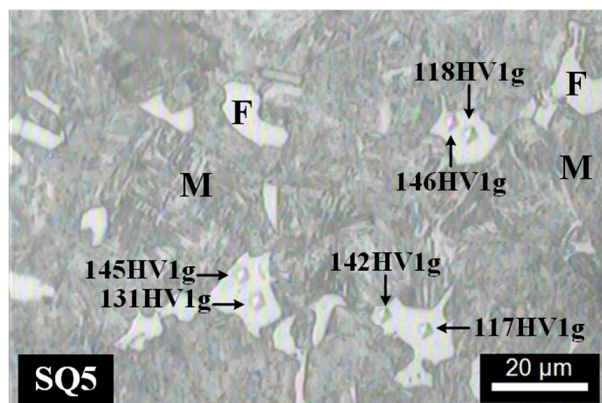


Figure 4. Typical light micrograph with superimposed locations at which ferrite microhardness tests were carried out and the associated ferrite microhardness data showed the alteration of ferrite hardening within the specific ferrite grains recorded on heat-treated SQ5 ferrite-martensite DP specimens. A greater ferrite hardening response was realized in the areas adjacent to the martensite in contrast to the central areas of ferrite grains. The ferrite microhardness data are measured with a fixed loading force of 1 g. F: Ferrite; M: Martensite [25].

3.3. Alloying Element Partitioning between Ferrite and Prior Austenite

3.3.1. Spot EDS Analysis for Alloying Concentration

The EDS analysis was accomplished widely at several positions within central ferrite grains and the central vicinity martensite (prior austenite) regions in order to investigate in detail the alteration of carbon, Si, Cr and Mn partitioning within ferrite and prior austenite regions developed during the progress of ferrite formation at 720 °C using various SQ heat-treated samples. Although, the measurement of carbon concentration within ferrite and prior austenite (martensite) microphases by EDS analysis technique accompanied some overestimation, but this technique can still be used as a comparable study in order to identify the alteration of carbon concentration within ferrite and prior austenite microphases as reported by several investigators [7,26,27]. In this way, the results of spot EDS analysis for carbon, Si, Cr, and Mn concentrations within the central locations of ferrite and martensite microphases are summarized in Tables 3 and 4 for various SQ heat-treated samples. For a better comparison of carbon, Si, Cr and Mn partitioning within ferrite and prior austenite with the progress of ferrite formation at 720 °C, the concentrations of these alloying elements as a function of SQ holding times are shown in Figure 5 for central ferrite and martensite areas. A careful investigation of the results depicted in Table 3 and Figure 5a illustrates that the mean level of carbon concentration within the central region of ferrite grains decreased continuously from 6.32 EDSNs for the short time ferrite-martensite SQ1 samples to 5.87 EDSNs for the long time ferrite-pearlite ones in conjunction with a concomitant increase in carbon concentration of prior austenite from 10.64 to 11.87 EDSNs, respectively. These qualitative results illustrate that a higher level of carbon concentration occurred within the prior austenite regions associated with the pearlite formation (SQ30) as a consequence of greater ferrite areas, in comparison to the prior austenite formation related to the short time treated SQ1 specimens. The Si concentration within the central areas of ferrite grains increased with a gentle slope from 1.23 to 1.51 EDSNs, while this was almost constant for the central location of prior austenite areas (Figure 5b, Table 3). The mean Cr concentration also increased within the central ferrite grain from 0.83 to 1.09 EDSNs with the increase in SQ holding times from 1 to 30 min (Figure 5c, Table 4). However, the amount of mean Cr concentration in the central region of martensite areas did not change for the SQ1, SQ5, and SQ15 samples with ferrite-martensite microstructures (nearly 0.93 EDSNs), while it increased suddenly to 1.25 EDSNs for the SQ30 sample with ferrite-pearlite microstructures. These results indicate that Si and Cr atoms are partitioned from growing ferrite-prior austenite interfaces towards the ferrite phase constituents during the progress of ferrite formation, and Cr atoms, on the other hand, promote pearlite formation

at the lateral stages of prior austenite phase transformation in SQ30 specimens heat treated for the prolonged duration. Although, the Mn content of central ferrite grains has been almost constant, the amount of mean Mn concentration increased in the central region of martensite areas from 0.50 to 0.72 EDSNs with the increase in SQ holding time from 1 to 15 min. For longer isothermal holding of 30 min, the amount of mean Mn concentration within the central region of pearlite increased to 0.78 EDSNs, emphasizing that Mn atoms did partition to the prior austenite side during the progress of ferrite formation in the SQ heat-treated specimens (Figure 5d, Table 4).

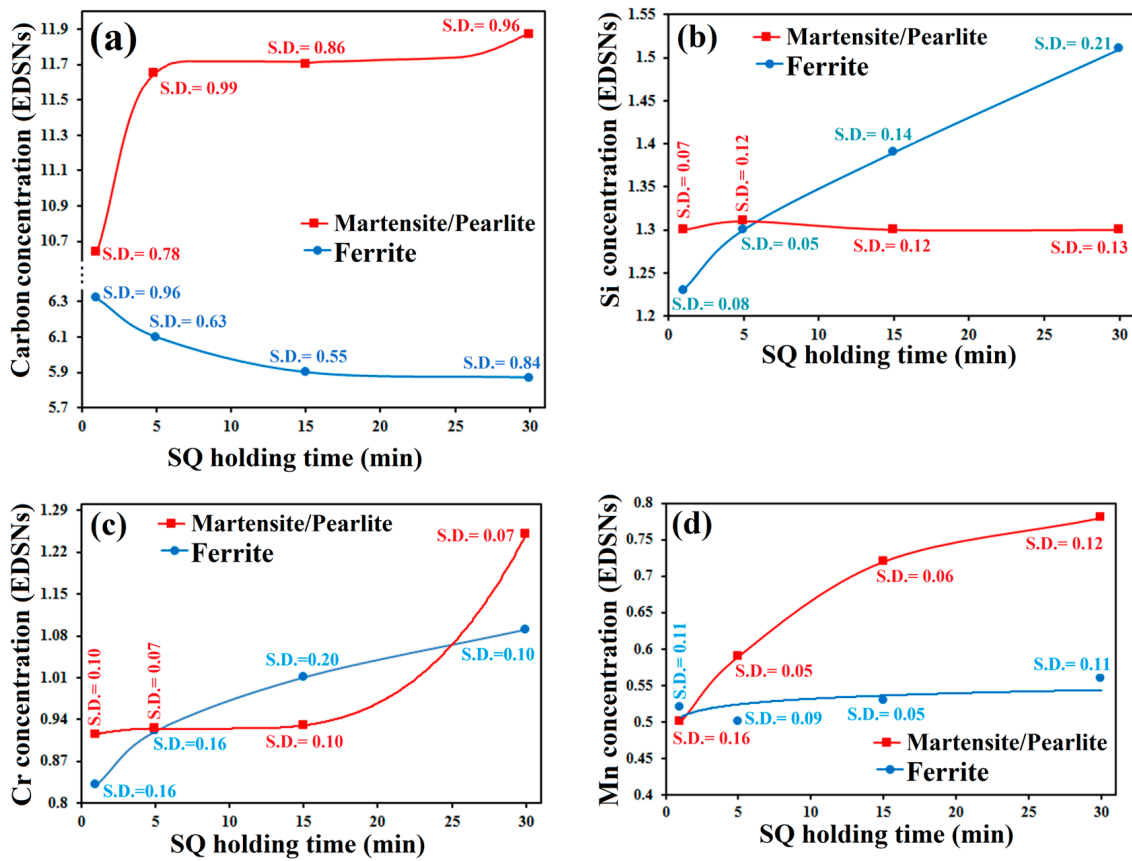


Figure 5. Changes in carbon (a), Si (b), Cr (c), and Mn (d) concentrations as a function of SQ holding time for central regions of ferrite and martensite/pearlite areas using various SQ heat-treated samples.

Table 3. The results of mean EDS analysis with the related average (Ave.) and standard deviation (S.D.) for carbon and Si concentrations within the central regions of ferrite grains and martensite areas taken from various SQ heat-treated samples.

Sample Mark	Carbon Content (EDSNs)				Si Content (EDSNs)			
	Ferrite		Martensite		Ferrite		Martensite	
	Ave.	S.D.	Ave.	S.D.	Ave.	S.D.	Ave.	S.D.
SQ1	6.32	0.96	10.64	0.78	1.23	0.08	1.30	0.07
SQ5	6.10	0.63	11.67	0.99	1.30	0.05	1.32	0.12
SQ15	5.90	0.55	11.69	0.86	1.39	0.14	1.30	0.12
			Pearlite				Pearlite	
SQ30	5.87	0.84	11.87	0.96	1.51	0.21	1.30	0.13

Table 4. The results of mean EDS analysis with the related average (Ave.) and standard deviation (S.D.) for Cr and Mn concentrations within the central regions of ferrite grains and martensite areas taken from various SQ heat-treated samples.

Sample Mark	Cr Content (EDSNs)				Mn Content (EDSNs)			
	Ferrite		Martensite		Ferrite		Martensite	
	Ave.	S.D.	Ave.	S.D.	Ave.	S.D.	Ave.	S.D.
SQ1	0.83	0.16	0.92	0.10	0.52	0.11	0.50	0.16
SQ5	0.92	0.16	0.93	0.07	0.50	0.09	0.59	0.05
SQ15	1.01	0.20	0.93	0.10	0.53	0.05	0.72	0.06
			Pearlite				Pearlite	
SQ30	1.09	0.10	1.25	0.07	0.56	0.11	0.78	0.12

3.3.2. Line Scan EDS Analysis for Alloying Concentration

To study the ferrite hardening mechanisms and related possibility of solid solution hardening effects of carbon and other alloying elements, the EDS line scan analyses were accomplished at various positions of ferrite grains as illustrated in Figure 6. The general microstructures of short (SQ5) and long time (SQ30) treated samples are depicted by electron micrographs presented in Figure 6a,b, respectively. The associated results of EDS analyses for C, Si, Cr, and Mn concentrations across the ferrite grains are illustrated in Figure 6a₁–a₄,b₁–b₄ taken from short (SQ5) and long time (SQ30) treated specimens, respectively. The carbon concentration from the central position of ferrite grains toward the ferrite area adjacent to the ferrite-prior austenite interfaces increased from 5.13 to 7.25 and 3.85 to 10.35 EDSNs, as respective SQ holding time increased from 5 to 30 min (Figure 6a₁,b₁). These results show that the prior austenite to ferrite phase transformation was related to a greater carbon concentration within ferrite areas formed at pre-existing defect regions of prior austenite grain boundaries and that the progress of ferrite formation was accompanied by further carbon rejection from ferrite to the remaining austenite regions, causing a considerable gradient in the carbon concentration across ferrite grains. The Si concentration from the ferrite region close to the ferrite-prior austenite interfaces, towards the central location of ferrite grains, increased from 1.12 to 1.44 and 1.07 to 1.54 EDSNs (Figure 6a₂,b₂), and also the Cr concentration increased from 0.78 to 1.00 and 0.75 to 1.11 EDSNs, with respective SQ holding time increasing from 5 to 30 min (Figure 6a₂,a₃,b₂,b₃). These results illustrate that Si and Cr atoms are distributed from the growing ferrite-prior austenite interfaces towards the ferrite grains. The Mn concentration, on the other hand, increased from 0.44 to 0.73 and 0.51 to 0.78 EDSNs for central locations of ferrite grains towards the ferrite regions adjacent to the ferrite-prior austenite interfaces of SQ5 and SQ30 samples, respectively (Figure 6a₄,b₄). The higher carbon and Mn concentrations of ferrite areas close to the ferrite-prior austenite areas can be associated to the considerable contribution of solid solution hardening for these ferrite regions.

3.4. Ferrite/Martensite Residual Stress Analysis

Typical XRD analysis has been employed to detect and estimate the microstructural microconstituents and the associated results are shown in Figure 7 for various SQ heat-treated specimens. All the patterns show almost the same BCC diffracted ferrite/martensite planes emphasizing that the peaks corresponding to ferrite or martensite microphases occurred in the same diffracted angles and it is typically difficult to distinguish between martensite and ferrite by XRD analysis because of low tetragonality of martensite developed in this low carbon low alloy steel. Approximately very small peaks of retained austenite (RA) can be also detected for ferrite-martensite DP specimens.

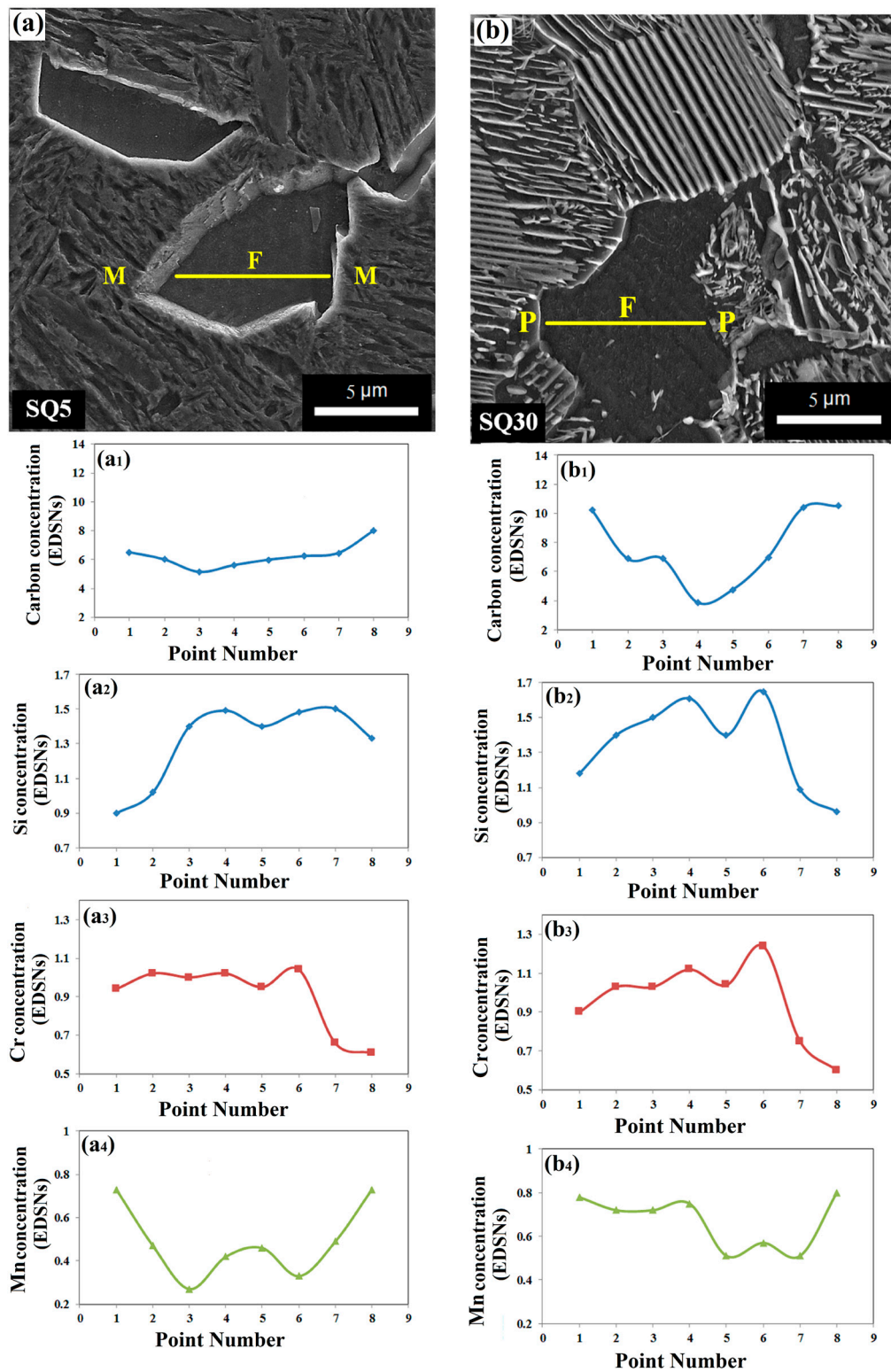


Figure 6. Electron micrographs along with carbon, Si, Cr and Mn EDS line-scan curves taken from short (SQ5) and long time (SQ30) treated samples presented in (a,a₁–a₄) and (b,b₁–b₄); respectively. (a,b) represent electron micrographs in conjunction with hypothetical EDS scan lines expanded within ferrite grains followed in turn by (a₁–a₄); and (b₁–b₄) indicating the respective qualitative curves for carbon, Si, Cr and Mn concentrations within ferrite grains, respectively. Ferrite grains, pearlite and martensite are labeled as F, P and M symbols, respectively.

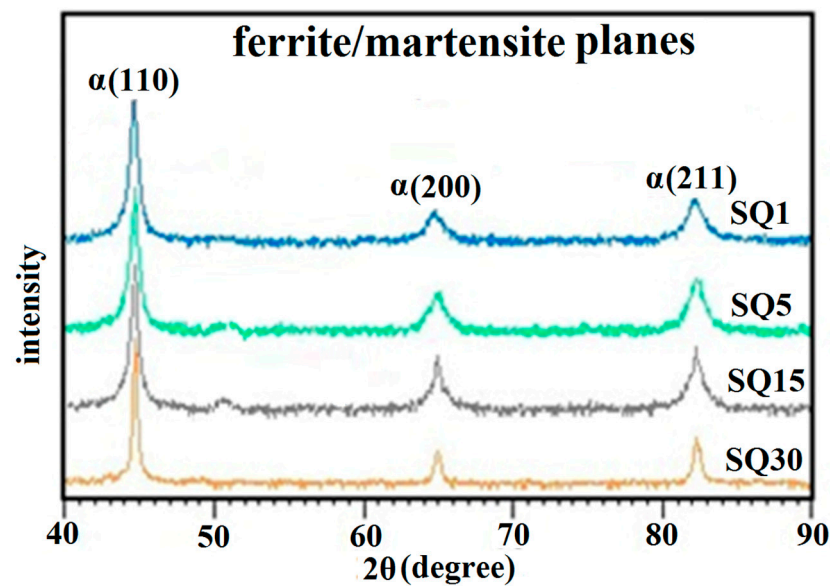


Figure 7. Comparison of XRD patterns of various SQ heat-treated specimens.

Residual stress “ $\text{Sin}^2\Psi$ ” analysis was carried out using the various (211) diffracted ferrite/martensite planes at Ψ angles including -30 , -20 , -10 , 0 , 15 , 30 and 45 deg from the XRD results shown in Figure 7. A ferrite/martensite peak was chosen for the analysis because of the compositional effects, such as solute carbon variation in the prior austenite, which could also cause shifting of ferrite/martensite peak. Figure 8 shows the variation in residual stress values calculated from the $\text{Sin}^2\Psi$ analysis results obtained from various SQ heat-treated specimens. For these calculations, $E \sim 177$ GPa and $\nu = 0.26$ were used [28]. From the $\text{Sin}^2\Psi$ analyses, it has been determined that the d-spacing decreases with increasing Ψ , indicating that ferrite/martensite is under higher residual compressive stress condition in short-time treated SQ specimens. This phenomenon can be correlated a higher mutual ferrite-martensite interaction, thereby generating a considerable density of geometrically necessary dislocations within lower ferrite containing SQ specimens. On the other hand, with increasing in SQ holding time at 720 °C, the progress of ferrite formation was enhanced, resulting in more recovered ferrite in the microstructures.

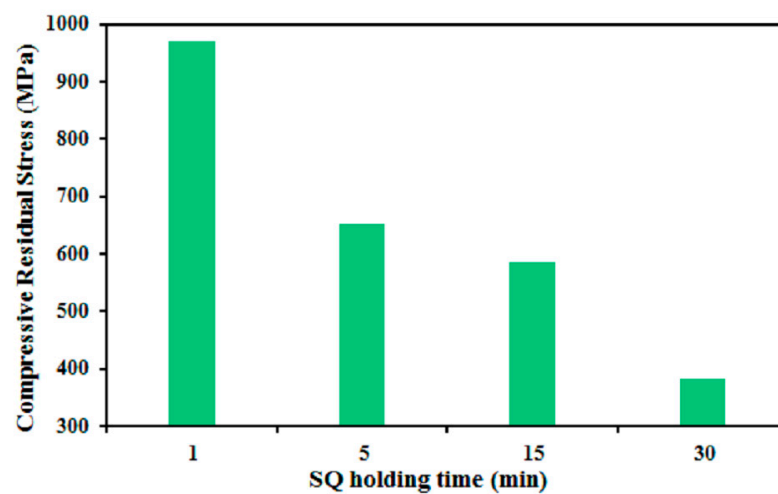


Figure 8. Compressive residual stress values (σ_ϕ) obtained from $\text{Sin}^2\Psi$ analyses versus SQ holding time.

3.5. Ferrite Hardening Mechanism

The experimental results indicate that not only the ferrite hardening is quite variable as a function of volume fraction of ferrite, but also it has changed across a specific ferrite grain (from central location towards the ferrite-martensite interfaces) for a particular SQ heat-treated sample (Figures 3 and 4). For ferrite-martensite DP samples containing large fractions of martensite, a significant contribution to ferrite hardening can be associated to the high level of carbon concentration and of course, residual compressive stresses extended within finer ferrite grains (Table 3, Figures 5a and 8). Fine ferrite grains with high carbon concentrations indicate that in addition to the other ferrite hardening mechanisms such as refinement of ferrite crystallite size as well as ferrite-martensite interaction, the solid solution hardening effect of C should be considered to account for the variations in ferrite hardness of short-time treated SQ specimens. Ferrite grains with higher carbon concentrated will have inevitable occurrence of lattice distortion and creation of stress field around solute iron atoms that can be contributed in part to the higher mechanical behavior of ferrite in the ferrite-martensite DP samples containing higher martensite volume fraction. On the other hand, it is obvious that the comprehensive partitioning of carbon will be faster at ferrite-prior austenite interfacial regions with significant density of defects. This is accompanied by the progress of prior austenite to ferrite phase transformation that can be associated to the possibility of greater segregation of carbon atoms to the induced dislocations as well as increased interaction of iron atoms with its stress fields leading to a greater capability to constrain the mobility of geometrically necessary dislocations, which raises the ferrite resistance to deformation through solid solution hardening mechanism [29,30].

The higher ferrite hardening in SQ heat-treated samples containing lower volume fraction of ferrite can be made according to the enhanced interaction of martensite with fine ferrite grains generating higher residual compressive stresses within ferrite (Figure 8). The formation of greater martensite volume fraction in the short-time treated SQ samples means that a smaller ferrite crystallite size is often surrounded by greater numbers of martensitic packets. As a result, the lower fraction of an individual ferrite grain in the short-time treated ferrite-martensite SQ samples experiences a higher localized compressive residual stresses in comparison with the long-time treated ferrite-martensite SQ samples, and hence, the ferrite hardness increases because of the lower mean spacing between dislocations [15,31,32]. This ferrite hardening mechanism seems to be more and more effective in the ferrite-martensite DP specimens containing a higher volume fraction of martensite, beside the occurrence of finer grain boundary ferrite crystals in comparison to the those of DP specimens containing lower volume fractions of martensite. Therefore, it is reasonable to conclude that the short-time treated SQ specimens are characterized by a higher density of dislocations caused by shear and extensive strain generated by the associated martensitic phase transformation, since this path is expected to minimize the accommodation strain energy for the formation of ferrite-martensite interfaces [33,34].

An abnormal trend in ferrite microhardness data occurred in respect of ferrite formation in the case of prolonged-time treated ferrite-pearlite SQ30 samples in comparison to the ferrite-martensite DP microstructures of shorter-time treated SQ samples (Figure 3c). This is interesting to emphasize that an abnormal high ferrite hardness occurred in the SQ30 heat-treated samples containing the maximum level of 15% ferrite with lower carbon concentration in association with the remaining 85% soft pearlite regions. These results indicate that the abnormal ferrite hardening cannot be related to the solid solution hardening effect of carbon and ferrite-martensite interaction, and that this ferrite hardening phenomenon can be associated to a higher redistribution of Si and Cr atoms within ferrite as shown in Figure 9. The Si and Cr concentrations within the central regions of ferrite grains increased by gentle slopes comprising 1.39 to 1.51 and 1.01 to 1.09 EDSNs, respectively, as the SQ holding time increased from 15 to 30 min, while the Si and Cr concentrations were almost constant for the central martensite areas. Therefore, intense solid solution hardening effects of Si and Cr atoms would give rise to the greater hardening of resultant ferrite crystals in the prolonged-time treated SQ30 samples (Figures 3c and 9).

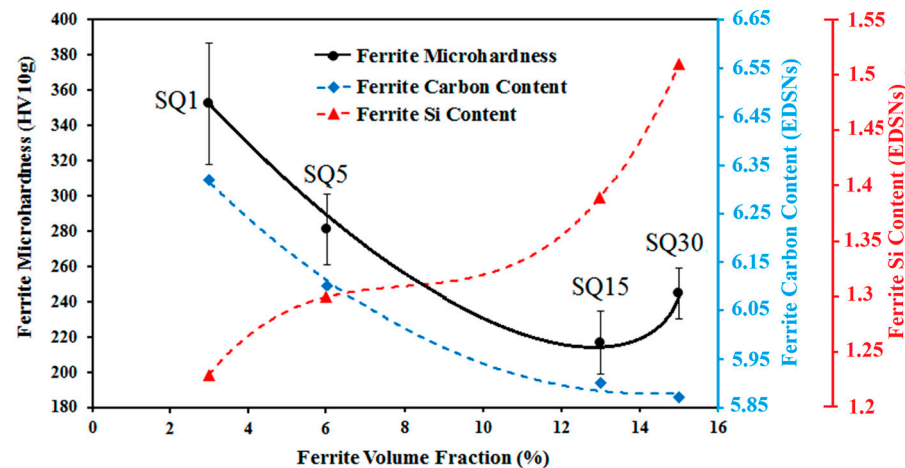


Figure 9. Changes in ferrite microhardness, ferrite carbon content and ferrite Si content as a function of progress of ferrite formation for the various SQ heat treated samples.

In addition to a greater solid solution hardening effect caused by relatively higher carbon concentration in ferrite areas adjacent to the ferrite-prior austenite interfaces, the corresponding higher ferrite hardness can also be in part related to the prior austenite to martensite phase transformation causing localized higher residual compressive stresses within adjacent ferrite regions. This is due to the generation of a high dislocation density within ferrite, following water quenching from 720 °C to room temperature. The accommodation of compressive residual stresses generated during prior austenite to martensite phase transformation can also be related to the generation of a greater level of mobile dislocation in the vicinity of ferrite areas leading to a greater magnitude of ferrite microhardness that increases from the central position toward the interfacial ferrite regions [35–37]. Therefore, besides uneven partitioning of a greater concentration of carbon within ferrite region adjacent to martensite, the mutual ferrite-martensite interaction generating a considerable density of geometrically necessary dislocations within ferrite can be also considered to be responsible in part for the higher hardening of ferrite area close to the ferrite-martensite interfaces.

4. Conclusions

Ferrite hardening alteration was studied in a medium silicon low alloy commercial grade of 35CHGSA steel under ferrite-martensite/ferrite-pearlite microstructures in relation to possibility of carbon, Si, Cr and Mn partitioning between ferrite and prior austenite microphases over a wide range of ferrite volume fractions. The conclusions are as followings:

1. The prior austenite to ferrite phase transformation has proceeded consistently with increase in SQ holding time at 720 °C. By increasing of SQ holding time from 1 to 30 min, the volume fraction of ferrite increased from 3% to a maximum value of 15%, respectively.
2. Both ferrite-martensite and ferrite-pearlite DP microstructures were realized during SQ holding time extending over 30 min at 720 °C. For SQ holding time lower than 15 min, only the ferrite-martensite DP microphases formed in the microstructures, while a mixture of ferrite and pearlite microphase constituents were realized in the prolonged-time treated SQ30 samples.
3. The ferrite hardening is completely variable with volume fraction of ferrite in the SQ samples. At first, the average ferrite microhardness sharply decreased from 352 to 217HV5g with the increase in volume fraction of ferrite from 3 to 13% under ferrite-martensite DP microstructures, respectively. Then, the average ferrite microhardness was abnormally higher from its lowest value of 217HV5g corresponding to the ferrite volume fraction of 13%, to 245HV5g with a marginal increase in ferrite volume

fraction to 15%, but with remaining fraction comprising of pearlite in SQ30 heat-treated samples.

4. A significant alteration in ferrite hardening also occurred within a given ferrite grain of a particular ferrite-martensite DP microstructure. The ferrite microhardness increased from 122 to 145HV1g with increasing distance from the central ferrite areas toward the ferrite-martensite interfaces of coarse ferrite grains realized in the SQ5 samples.
5. In contrast to almost constant Mn content of ferrite, the average Si and Cr concentrations for ferrite grains increased along gentle slopes from 1.23 to 1.51 and 0.83 to 1.09 EDSNs, respectively, with SQ holding time increasing from 1 to 30 min, respectively. The further intense solid solution hardening effects of Si and Cr would give rise to the abnormally greater hardening of resultant ferrite grains in the prolonged-time treated SQ30 samples.
6. The carbon concentration of ferrite is completely variable depending on the progress of ferrite formation. The average ferrite carbon concentration diminished from 6.32 to 5.90EDSNs with raising SQ holding time from 1 to 15 min, respectively. The average carbon concentration has also increased from 5.13 to 7.25EDSNs as the indentation location was moved from the central locations of ferrite grains towards the regions adjacent to the ferrite-prior austenite interfaces of SQ5 samples. The higher carbon concentration can be related to the more solid solution hardening of ferrite.
7. The residual compressive stresses decreased from 971 to 382 MPa with the increase in SQ holding time from 1 to 30 min at 720 °C. The higher residual compressive stresses of short time treated SQ specimens are associated in part to the higher ferrite hardening of large martensite containing DP microstructures.

Author Contributions: Conceptualization, S.S.G.B., S.A.S. and M.C.S.; methodology, S.S.G.B., S.A.S. and M.C.S.; software, A.K.; validation, A.K.; formal analysis, A.K. and S.S.G.B.; investigation, A.K.; resources, A.K., S.S.G.B., S.A.S. and M.C.S.; data curation, A.K. and S.S.G.B.; writing—original draft preparation, A.K. and S.S.G.B.; writing—review and editing, A.K., S.S.G.B. and M.C.S.; visualization, A.K. and M.C.S.; supervision, A.K.; project administration, S.S.G.B.; funding acquisition, S.S.G.B. and M.C.S.; All authors have read and agreed to the published version of the manuscript.

Funding: This research received no external funding.

Acknowledgments: One of the authors, M.C. Somani, would like to express his gratitude to the Academy of Finland for funding this research under the auspices of the Genome of Steel (Profi3) through project #311934.

Conflicts of Interest: The authors declare no conflict of interest.

References

1. Gaggiotti, M.; Albini, L.; Di Nunzio, P.E.; Di Schino, A.; Stornelli, G.; Tiracorrendo, G. Ultrafast Heating Heat Treatment Effect on the Microstructure and Properties of Steels. *Metals* **2022**, *12*, 1313. [[CrossRef](#)]
2. Abedini, O.; Behroozi, M.; Marashi, P.; Ranjbarnodeh, E.; Pouranvari, M. Inter-critical heat treatment temperature dependence of mechanical properties and corrosion resistance of dual phase steel. *Mater. Res.* **2019**, *22*, 1–10. [[CrossRef](#)]
3. Alipour, M.; Torabi, M.A.; Sareban, M.; Lashini, H.; Sadeghi, E.; Fazaeli, A.; Habibi, M.; Hashemi, R. Finite element and experimental method for analyzing the effects of martensite morphologies on the formability of DP steels. *Mech. Based Des. Struct. Mach.* **2020**, *48*, 525–541. [[CrossRef](#)]
4. Ko, Y.G.; Lee, C.W.; Namgung, S.; Shin, D.H. Strain hardening behavior of nanostructured dual-phase steel processed by severe plastic deformation. *J. Alloy. Compd.* **2010**, *504*, 452–455. [[CrossRef](#)]
5. Mulidrán, P.; Spišák, E.; Tomáš, M.; Majerníková, J.; Bidulská, J.; Bidulský, R. Impact of Blank Holding Force and Friction on Springback and Its Prediction of a Hat-Shaped Part Made of Dual-Phase Steel. *Materials* **2023**, *16*, 811. [[CrossRef](#)]
6. Schino, A.D. Analysis of phase transformation in high strength low alloyed steels. *Metalurgija* **2017**, *56*, 349–352.
7. Wang, C.; Shi, J.; Cao, W.; Dong, H. Characterization of microstructure obtained by quenching and partitioning process in low alloy martensitic steel. *Mater. Sci. Eng. A* **2010**, *527*, 3442–3449. [[CrossRef](#)]
8. Kumar, A.; Singh, S.B.; Ray, K. Influence of bainite/martensite-content on the tensile properties of low carbon dual-phase steels. *Mater. Sci. Eng. A* **2008**, *474*, 270–282. [[CrossRef](#)]

9. Ashrafi, H.; Shamanian, M.; Emadi, R.; Saeidi, N. Correlation of tensile properties and strain hardening behavior with martensite volume fraction in dual-phase steels. *Trans. Indian Inst. Met.* **2017**, *70*, 1575–1584. [[CrossRef](#)]
10. Khajesarvi, A.; Ghasemi Banadkouki, S.S.; Sajjadi, S.A. Effect of tempering heat treatment on mechanical properties of a medium silicon low alloy ferrite–martensite DP steel. *Int. J. Iron Steel Soc. Iran* **2022**, *19*, 20–29.
11. Bag, A.; Ray, K.; Dwarakadasa, E. Influence of martensite content and morphology on the toughness and fatigue behavior of high-martensite dual-phase steels. *Metall. Mater. Trans. A* **2001**, *32*, 2207–2217. [[CrossRef](#)]
12. Bag, A.; Ray, K.; Dwarakadasa, E. Influence of martensite content and morphology on tensile and impact properties of high-martensite dual-phase steels. *Metall. Mater. Trans. A* **1999**, *30*, 1193–1202. [[CrossRef](#)]
13. Cai, X.-L.; Feng, J.; Owen, W. The dependence of some tensile and fatigue properties of a dual-phase steel on its microstructure. *Metall. Trans. A* **1985**, *16*, 1405–1415. [[CrossRef](#)]
14. Peng-Heng, C.; Preban, A. The effect of ferrite grain size and martensite volume fraction on the tensile properties of dual phase steel. *Acta Metall.* **1985**, *33*, 897–903. [[CrossRef](#)]
15. Kadkhodapour, J.; Schmauder, S.; Raabe, D.; Ziaei-Rad, S.; Weber, U.; Calcagnotto, M. Experimental and numerical study on geometrically necessary dislocations and non-homogeneous mechanical properties of the ferrite phase in dual phase steels. *Acta Mater.* **2011**, *59*, 4387–4394. [[CrossRef](#)]
16. Byun, Y.S.; KIM, I.S.; KIM, S.J. Yielding and Strain Aging Behaviors of an Fe-0.07 C-1.6 Mn Dual-phase Steel. *Trans. Iron Steel Inst. Jpn.* **1984**, *24*, 372–378. [[CrossRef](#)]
17. Jiang, Z.; Guan, Z.; Lian, J. The relationship between ductility and material parameters for dual-phase steel. *J. Mater. Sci.* **1993**, *28*, 1814–1818. [[CrossRef](#)]
18. Ebrahimi, A.; Banadkouki, S.G. Effect of alloying element partitioning on ferrite hardening in a low alloy ferrite-martensite dual phase steel. *Mater. Sci. Eng. A* **2016**, *677*, 281–289. [[CrossRef](#)]
19. Monia, S.; Varshney, A.; Sangal, S.; Kundu, S.; Samanta, S.; Mondal, K. development of highly ductile spheroidized steel from high C (0.61 wt.% C) low-alloy steel. *J. Mater. Eng. Perform.* **2015**, *24*, 4527–4542. [[CrossRef](#)]
20. *Astm E3-01*; Standard Guide for Preparation of Metallographic Specimens. Testing, American Society for and Materials, Astm: West Conshohocken, PA, USA, 2009.
21. Vander Voort, G.F. *Metallography and Microstructures*; ASM International Materials Park: Geauga County, OH, USA, 2004; Volume 9.
22. HE, J.; Schoenung, J. *ASTM E-562-02-Standard Test Method for Determining Volume Fraction by Systematic Manual Point*; American Society for Testing and Materials: West Conshohocken, PA, USA, 2005; Volume 3.
23. Cullity, B.D. *Elements of X-Ray Diffraction*; Addison: Wesley, MA, USA, 1978; pp. 127–131.
24. Noyan, I.C.; Cohen, J.B.; Noyan, I.C.; Cohen, J.B. Determination of strain and stress fields by diffraction methods. *Residual Stress Meas. Diffr. Interpret.* **1987**, *1*, 117–163.
25. Khajesarvi, A.; Banadkouki, S.S. Investigation of carbon and silicon partitioning on ferrite hardening in a medium silicon low alloy ferrite-martensite dual-phase steel. *Int. J. Iron Steel Soc. Iran* **2020**, *17*, 25–33.
26. Zarchi, H.R.K.; Khajesarvi, A.; Banadkouki, S.S.G.; Somani, M.C. Microstructural evolution and carbon partitioning in interstitial free weld simulated api 5l x60 steel. *Rev. Adv. Mater. Sci.* **2019**, *58*, 206–217. [[CrossRef](#)]
27. Soleimani, M.; Mirzadeh, H.; Dehghanian, C. Processing route effects on the mechanical and corrosion properties of dual phase steel. *Met. Mater. Int.* **2020**, *26*, 882–890. [[CrossRef](#)]
28. Mizubayashi, H.; Yumoto, S.; Li, H.; Shimotomai, M. Young's modulus of single phase cementite. *Scr. Mater.* **1999**, *40*, 773–777. [[CrossRef](#)]
29. Li, Y.; Li, W.; Min, N.; Liu, H.; Jin, X. Homogeneous elasto-plastic deformation and improved strain compatibility between austenite and ferrite in a co-precipitation hardened medium Mn steel with enhanced hydrogen embrittlement resistance. *Int. J. Plast.* **2020**, *133*, 102805. [[CrossRef](#)]
30. Cong, J.; Li, J.; Fan, J.; Misra, R.D.K.; Xu, X.; Wang, X. Effect of austenitic state before ferrite transformation on the mechanical behavior at an elevated temperature for seismic-resistant and fire-resistant constructional steel. *J. Mater. Res. Technol.* **2021**, *13*, 1220–1229. [[CrossRef](#)]
31. Calcagnotto, M.; Ponge, D.; Demir, E.; Raabe, D. Orientation gradients and geometrically necessary dislocations in ultrafine grained dual-phase steels studied by 2D and 3D EBSD. *Mater. Sci. Eng. A* **2010**, *527*, 2738–2746. [[CrossRef](#)]
32. Sodjit, S.; Uthaisangskuk, V. Microstructure based prediction of strain hardening behavior of dual phase steels. *Mater. Des.* **2012**, *41*, 370–379. [[CrossRef](#)]
33. Morooka, S.; Tomota, Y.; Kamiyama, T. Heterogeneous deformation behavior studied by in situ neutron diffraction during tensile deformation for ferrite, martensite and pearlite steels. *ISIJ Int.* **2008**, *48*, 525–530. [[CrossRef](#)]
34. Calcagnotto, M.; Adachi, Y.; Ponge, D.; Raabe, D. Deformation and fracture mechanisms in fine-and ultrafine-grained ferrite/martensite dual-phase steels and the effect of aging. *Acta Mater.* **2011**, *59*, 658–670. [[CrossRef](#)]
35. Jacques, P.; Furnémont, Q.; Mertens, A.; Delannay, F. On the sources of work hardening in multiphase steels assisted by transformation-induced plasticity. *Philos. Mag. A* **2001**, *81*, 1789–1812. [[CrossRef](#)]

36. Erdogan, M.; Priestner, R. Effect of epitaxial ferrite on yielding and plastic flow in dual phase steel in tension and compression. *Mater. Sci. Tech.* **1999**, *15*, 1273–1284. [[CrossRef](#)]
37. Ostash, O.; Kulyk, V.; Poznyakov, V.; Haivorons'kyi, O.; Markashova, L.; Vira, V. Fatigue crack growth resistance of welded joints simulating the weld-repaired railway wheels' metal. *Arch. Mater. Sci. Eng.* **2017**, *86*, 49–55. [[CrossRef](#)]

Disclaimer/Publisher's Note: The statements, opinions and data contained in all publications are solely those of the individual author(s) and contributor(s) and not of MDPI and/or the editor(s). MDPI and/or the editor(s) disclaim responsibility for any injury to people or property resulting from any ideas, methods, instructions or products referred to in the content.